

---

## Short-wave instability growth in closely spaced vortex pairs

---

Nicholas Boustead\*, Kris Ryan  
and Gregory J. Sheard

Fluids Laboratory for Aeronautical and Industrial Research (FLAIR),  
Department of Mechanical and Aerospace Engineering,  
Monash University, VIC 3800, Australia  
Fax: 61 3 9905 1825

E-mail: Nicholas.boustead@monash.edu

E-mail: Kris.Ryan@monash.edu

E-mail: Greg.Sheard@monash.edu

\*Corresponding author

**Abstract:** The growth of short-wave elliptical instabilities in a Lamb-Oseen vortex pair subject to non-uniform strain fields at close vortex spacing is considered using direct numerical simulation at a Reynolds number  $Re = 20000$ . A linear stability analysis demonstrates that with reduced vortex spacing the growth rate of all axial wave-numbers is enhanced relative to that of the fastest-growing mode. A coupling of vortices is observed at close vortex spacing, which may lead to improved non-linear instability growth, and the development of fluid cross-over regions. These fluid cross-over regions are shown to be products of a linear growth regime.

**Keywords:** elliptic instability; growth rate; Lamb-Oseen; vortex pair; linear stability analysis; fluid cross-over; aircraft wakes.

**Reference** to this paper should be made as follows: Boustead, N., Ryan, K. and Sheard, G.J. (2010) 'Short-wave instability growth in closely spaced vortex pairs', *Progress in Computational Fluid Dynamics*, Vol. 10, Nos. 5/6, pp.276–283.

**Biographical notes:** Nicholas Boustead is currently completing his PhD, which he commenced in 2009 working with the Fluids Laboratory for Aeronautical and Industry Research group (FLAIR) at Monash University, Melbourne, Australia. With this group he studies fluid dynamic systems, including aircraft wakes and fluid-structure interactions such as those found in biological flows.

Kris Ryan received his PhD in 2005 from Monash University, Melbourne, Australia. He is presently employed as a Senior Lecturer in the Department of Mechanical and Aerospace Engineering, Monash University, where he specialises in applying computational fluid dynamics algorithms to investigate aircraft wakes, biological flows, bio-mimetic propulsion devices and bluff body fluid interactions.

Gregory J. Sheard received his PhD in 2004 from Monash University, Melbourne, Australia. He is presently employed as a Senior Lecturer in the Faculty of Engineering, Monash University, where he specialises in the development and application of high-order computational fluid dynamics algorithms to problems spanning biological flows through to planetary atmospheric dynamics, and has published over 40 papers in both journals and international conference proceedings.

---

### 1 Introduction

The study of vortex dynamics is pivotal to the aviation industry in which the generation of large-scale, coherent vortices at the wingtips of large aircraft can present a significant hazard to aircraft downstream, where air flows are not uniform (Spalart, 1998). In order to maintain safety, a minimum distance between aircraft utilising a single runway must be maintained (Olwi and Ghazi, 1992). This minimum distance requirement imposes an upper limit

on the number of aircraft which may safely use airport facilities over a given period of time (Spalart, 1998).

The past 40 years has witnessed considerable research effort to understand the fundamental nature of aircraft wakes with an aim to enhance the dissipation of the strong, coherent vortical structures within them (Spalart, 1998). Crow (1970) identified a long-wavelength perturbation mechanism which led to the enhanced dissipation of coherent aircraft wakes. Despite the Crow instability mechanism's ability to induce vortex annihilation 20 times

faster than viscous dissipation alone, the long-wavelength instability still requires significant time to develop.

In the wakes of aircraft, elliptic instabilities are expected to influence the dynamics of the multiple vortices generated by aircraft wings. Each vortex is in the strain field generated by the surrounding vortices and, therefore, subjected to an elliptic instability. Leweke and Williamson (1998) showed the addition of a shortwave instability increased the instability growth rate by 20%.

The elliptic instability has been identified and studied in various contexts, ranging from three dimensional transition in shear flows (Bayly et al., 1988) to vortex interactions (Leweke and Williamson, 1998) and flows in elliptic containers (Eloy et al., 2003). Pierrehumbert (1986) and Bayly (1986), who considered the local stability properties of an elliptic flow, were the first to identify the generic aspects of the elliptical instability. Before these local analyses, Moore and Saffman (1975), and Tsai and Widnall (1976) had identified an instability which develops in strained vortices. They performed the first global stability analysis of elliptic instability and provided an instability mechanism in terms of normal mode resonance.

In vortex pairs without an axial flow component, the elliptic instability has been observed experimentally in both co-rotating vortices (Meunier and Leweke, 2005) and counter-rotating vortices (Leweke and Williamson, 1998). It has been modelled using Moore and Saffman's approach in Le Dizes and Laporte (2002), who describe the capacity of paired vortices to exert reciprocal strain fields that elliptically deform each vortex core. Le Dizes and Verga (2002) identified three key parameters contributing to the elliptical deformation process: vortex steepness  $n$ , Reynolds number and separation ratio ( $a/b$ ). The vorticity profile is described by

$$\omega_0(r) = \exp(-r^{2n}), \quad (1)$$

where  $n$  is the vortex steepness and  $n = 1$  gives a Gaussian vortex, and  $\omega_0$  is the vorticity. Here, the Reynolds number is defined as

$$\text{Re} = \Gamma/\nu, \quad (2)$$

where  $\Gamma$  is the circulation and  $\nu$  is the kinematic viscosity. In addition, elliptical deformations are driven by the mutually induced strain field of the vortex core. At large separations the strain field near the partner vortex core may be assumed to be uniform; however, at closer separations the strain field is curved.

Sipp et al. (2000) also showed that the elliptical deformation proceeds regardless of the initial vorticity profile, relaxing the vortices to a unique Gaussian state which is independent of the Reynolds number. This validates the use of a Lamb-Oseen pair in examining elliptical instabilities.

## 2 Instability mode interaction and development

Leweke and Williamson (1998) concluded the elliptical instability of the two vortices evolves in a distinct phase relationship, breaking the initial symmetry of the pair. This they attribute to the coupling of instabilities, which produces an asymmetric mode to satisfy kinematic matching conditions. Leweke and Williamson's study also described the long-term evolution of the instability, demonstrating that the growing deformation of the short-wave instabilities gives rise to periodic cross-over of fluid between vortices. This creates an array of secondary vortices perpendicular to the primary pairs. The secondary vortices quickly lead to the breakdown of primary vortex circulation, as observed by Ryan and Sheard (2007). Leweke and Williamson proposed that the classical Crow instability is, in fact, the result of a long and short-wave instability interaction. They suggested that the long-wave instability causes vortex cores to exist closer in certain regions, leading to an increased growth rate of short-wave instabilities and, hence, secondary vortex formation in these regions.

The array of secondary vortices identified by Leweke and Williamson (1998) evolve in the non-linear growth phase of the  $[-1, 1]$  Kelvin mode. Ryan and Sheard (2007) demonstrated that the  $[-1, 1]$  Kelvin mode has the greatest dissipation rate for flows of this type as a result of production of secondary vortices. This is due to a non-linear growth zone of short-wave instabilities. A large growth rate during the linear phase proved insufficient to produce enhanced vortex dissipation in a Kelvin type mode (Kelvin modes are a classification scheme of instability modes). The numerical study employed may not have accounted for viscous diffusion, which moves the vortices closer together over time. This, in turn, may assist in the production of secondary vortices.

Previous analytical investigations that have established these instability relationships are only consistent when vortices are sufficiently separated so as to feel only a uniform strain field. Little is known about the propagation of short-wave instability modes at small vortex spacing (Le Dizes and Laporte, 2002). As such this investigation aims to:

- analyse the effects of short-wave elliptical instability modes on overall vortex pair evolution at small vortex spacing
- determine the effect of vortex spacing on the growth rate of the  $[-1, 1]$  instability mode
- identify any flow structures such as fluid crossover regions which may lead to the enhanced dissipation of the vortex pairs.

The current work will address these aims by performing a linear stability analysis on a Lamb-Oseen vortex pair. Previous work has been limited to a maximum vortex

separation ratio  $a/b = 0.25$ . This will be the lower limit of the determining parameter on the elliptical core deformation.

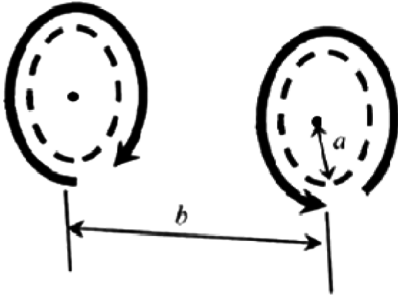
### 3 Flow field description

A pair of counter-rotating vortex pairs is created at the wing tips of aircraft as a product of the lift produced on the wings (Phillips, 2004). This investigation considers vortices of a Lamb-Oseen type (Fig. 1), which is a counter-rotating pair with Gaussian vorticity profile. The vorticity profile of the Lamb-Oseen vortex pair may be expressed mathematically by

$$\omega_z = \frac{\Gamma}{\pi a_0^2} e^{-r^2/a_0^2}, \quad (3)$$

where  $\omega_z$  is the axial vorticity component,  $a$  is the characteristic core radius of the vortex ( $a_0$  is the core radius at time  $t = 0$ ),  $\Gamma$  is the circulation and  $r$  is the radial position.

**Figure 1** Schematic representation of flow in a counter-rotating Lamb-Oseen pair with a Gaussian profile.  $a$  is the characteristic core radius,  $b$  is the separation distance



In this study, two counter-rotating Lamb-Oseen vortices, each of characteristic radius  $a$ , are placed a distance  $b$  apart. Each vortex imposes a weak external strain field on the other,  $e_0$  (for example see Le Dizes and Verga, 2002). This paper restricts its attention to the study of counter rotating vortices of equal circulation magnitude. The Lamb-Oseen vortex pair is characterised by a Gaussian vorticity profile which is a known global attractor of any two dimensional axisymmetric vortex (see for example Le Dizes and Verga, 2002). The Gaussian profile has the advantage over other possible profiles, because it is unaffected by viscous diffusion. Viscosity only acts to modify the radius of the vortex, which evolves linearly in time.

The amount the vortex core will diffuse is described by

$$a = \sqrt{a_0^2 + 4\nu t_1}, \quad (4)$$

where  $a_0$  is the initial vortex characteristic radius,  $t_1$  is the time taken to evolve this solution and  $\nu$  is the viscosity. And

$$t^* = \frac{t_1 \Gamma}{2\pi a_0^2}, \quad (5)$$

where  $t^*$  is the normalised time defined by Le Dizes and Verga (2002), and  $\Gamma$  is the circulation. Le Dizes and Verga

(2002) showed that a settling time of  $t^* = 40$  is sufficient for the vortices to adjust to the induced strain fields and form stable elliptical deformations.

The initial vortices were placed at the centre of a computational domain with vortex core radii of  $a = 0.97577$  and at a vortex spacing of  $b = 4a$  separation. At the conclusion of the settling time ( $t^* = 40$ ) the initial vortex spacing case of  $a/b = 0.25$  was formed. A Reynolds number  $Re = 20000$  will be used throughout the investigation. This is sufficient to ensure the effects of viscous diffusion are negligible throughout the analysis and, therefore, the vortex spacing remains constant.

### 4 Methodology

A spectral element technique is used to solve the incompressible Navier-Stokes equations

$$\frac{\partial u}{\partial t} + (u \cdot \nabla)u = -\nabla P + \nu \nabla^2 u, \quad (6a)$$

$$\nabla \cdot u = 0, \quad (6b)$$

where  $u$  is the velocity vector,  $\nabla$  is the gradient operator,  $P$  is a scalar pressure and  $t$  is time.

The package uses an operator splitting technique (Karniadakis et al., 1991), which allows the advection and diffusion terms to be solved independently for each time step. A spectral element method is used to discretise spatial terms. The domain is discretised into a series of macro elements, within which high-order tensor-product Lagrangian polynomials are employed as shape functions to solve the partial differential equations. A 3rd order accurate, backward multi-step method using a three-step splitting scheme evolves the solution in time to solve the linearised time dependent Navier-Stokes equations.

During the perturbation study, a disturbance of a single frequency is propagated in the vortex perpendicular to the 2D plane, acting along the axial direction of a vortex stream tube, allowing investigation of the susceptibility of the vortices to instabilities in the third dimension. To this end a global stability analysis is conducted in which the velocity and pressure fields ( $u \cdot p$ ) are broken up into a two dimensional base flow ( $\bar{U}, \bar{p}$ ) and a three dimensional disturbance ( $u', p'$ )

$$u = \bar{U} + u', \quad p = \bar{p} + p'. \quad (7a, b)$$

Substituting these into the Navier-Stokes equations, cancelling the base flow terms and neglecting products of the (small) perturbation field yields

$$\frac{\partial u'}{\partial t} + (\bar{U} \cdot \nabla)u' + (u' \cdot \nabla)\bar{U} = -\nabla P' + \nu \nabla^2 u'. \quad (8)$$

The stability analysis is then carried out simply by integrating the perturbation field forward in time and monitoring the growth or decay of the field. The perturbation field evolves over one period subject to an operator  $A$  as

$$u'_{n+1} = A(u'_n). \quad (9)$$

The eigenvalues of  $A$  correspond to linear growth multipliers of the system,  $\mu$ ,

$$\mu = e^{\sigma T}, \quad (10)$$

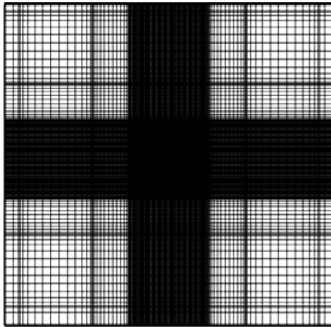
for which  $\sigma$  is the instability growth rate.

For further descriptions and validations of the two dimensional solver the reader is referred to Sheard et al. (2007). The linear stability analysis algorithm used in this study was extensively validated in Sheard et al. (2009) and was found to produce identical results to an independent implementation of the same algorithm in Blackburn and Sheard (2010).

## 5 Simulation optimisation

The mesh (Fig. 2) used in the vortex analysis consists of an internal fine region and a coarser outer region in which elements expand to the edge of the domain where the boundary conditions are applied. When created, the vortices exist in the centre of the refined region. This is where the vorticity is most concentrated and accuracy is most important.

**Figure 2** Mesh used in numerical investigation. The mesh consists of a central refined region and an outer coarse region. Elements shown include Gauss-Legendre-Lobatto points used in numerical quadrature



The two counter rotating vortices are created with a characteristic radius less than 1% of the computational domain width in all directions. Time-dependent Dirichlet boundary conditions are added at the boundaries of the domain, which apply a corrective velocity to keep the vortices positioned in the refined region of the mesh. The boundary is over 100 vortex radii from the vortex pair, which ensures the imposed boundary conditions do not adversely influence the underlying physics of the vortex interaction.

In order to optimise the accuracy of the grid a  $P$ -type grid resolution study was conducted. In this an  $L_2$ -norm and the vortex circulation were measured to assess the accuracy of the solution in a global context. The strain rate magnitude was assessed to determine the prevalence of noise in the solution in the core vortex region.

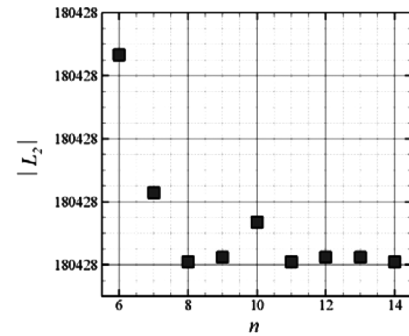
To measure the global accuracy of the flow field, two parameters were measured. Integration of the velocity field

over the domain provided an estimate of the vortex circulation, which may be compared to the input value. The second parameter was the  $L_2$ -norm, defined as

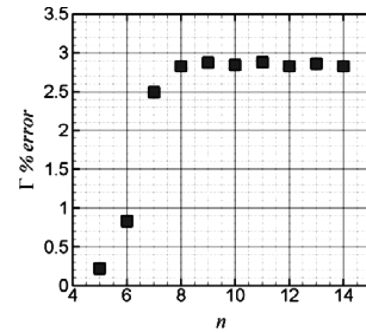
$$L_2 = \oint |u| d\Omega, \quad (11)$$

where  $|u|$  is the magnitude of the velocity vector and  $\Omega$  is the computational domain. Figure 3 shows that, in terms of the global accuracy of the solution, after the order of the polynomial used in the spectral solver exceeded 10 the solution converged to a consistent level of accuracy.

**Figure 3** Results from grid independence investigation: (a)  $L_2$ -norm and (b) estimation of the circulation through integral of velocity over half the computational domain, as a function of GLL polynomial degree  $n$



(a)



(b)

The strain rate magnitude, which is particularly sensitive to resolution, was measured at the vortex core. An element polynomial degree of 14 was found to resolve this quantity to high accuracy.

From the grid resolution study it was determined that a 14th degree polynomial was sufficient to provide a resolution independent result.

## 6 Base flow evolution

Le Dizes and Verga (2002) showed that vortices will grow larger in size over time, as a natural result of viscous diffusion (see Eq. 4).

Base flows of varying separation ratios were created using the viscous diffusion method employed by Le Dizes and Verga (2002). Lowering the Reynolds number to  $Re = 15\pi$  enhanced the effect of the viscous term in the Navier-Stokes equations. Given sufficient time the vortices

are allowed to diffuse, increasing the characteristic radius  $a$  and, thus, increasing the separation ratio. The flow structures created at different separations are shown in Figure 4. At small vortex separations there is significant elliptical deformation of the core. Figure 5 shows the strain fields of the largest separation case considered,  $a/b = 0.481$ . It can be clearly seen that the strain field is now curved within the vicinity of each vortex core. A fundamental assumption in analytical formulations such as those of Le Dizès and Laporte (2002) is that vortices were sufficiently separated such that a uniform strain field could be assumed at the core of each vortex.

**Figure 4** Vorticity profiles of vortex pairs: (a)  $a/b = 0.25$  and (b)  $a/b = 0.481$ . Solid lines represent positive vorticity, dashed lines are negative vorticity

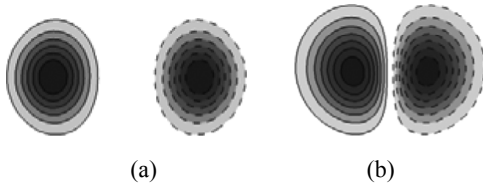
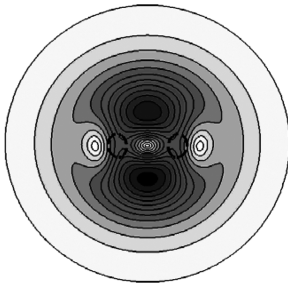


**Figure 5** Strain field at vortex separation 0.481. Note the curved nature of the strain field in the vicinity of the cores. The dashed circles indicate the locations of the vortex cores



### 7 Vortex spacing limit

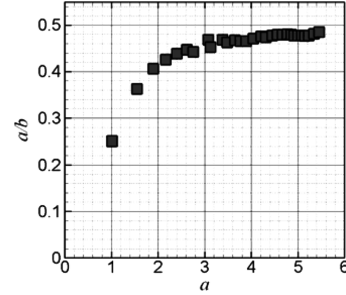
During the evolution of the vortex base flows an upper limit for the separation ratio was discovered. The vortex spacing was accurately determined using a Simpson’s 1/3rd quadrature method interpolating over the vortex region to find locations of maximum vorticity. The characteristic radius was determined using the axial vorticity  $\omega_0$  described by

$$\omega_0 = \frac{\Gamma}{\pi a^2} \exp\left(-\left(\frac{r}{a}\right)^2\right). \tag{12}$$

It was found that as the vortices grew closer, the strain field developed by each vortex pushed on the neighbouring vortex, forcing the pair apart. Figure 6 shows that an upper limit of  $a/b = 0.5$  for the vortex separation ratio. This implies that two vortices will never exist in the same space as defined by their characteristic core radii, i.e., their cores may never overlap. This also indicates that the strain field, while curved, will not permit periodic crossing of a shared vortex boundary. Given the majority of the

vorticity is contained within the characteristic core radius; we would not physically expect counter-rotating vortices to be able to violate this boundary without destruction of the vortex structure.

**Figure 6** Vortex separation ratio varying as a function of core radius  $a$



### 8 Perturbation study

A stability analysis was conducted on the vortex pair in which small disturbances were introduced of a specified axial wave-number. In this analysis the disturbance was evolved in a perturbation field, the effects of which may be observed by overlaying disturbance mode shape over the frozen base flow. Vortices of separation ratios  $a/b = 0.251, 0.3625, 0.4063, 0.4257, 0.4385,$  and  $0.447$  were investigated. Each was subject to a series of disturbances in the normalised wavelength range of  $\lambda/a = 0.2$  to  $5.0$ . Le Dizès and Laporte (2002) showed that this range is sufficient to describe the development of short-wavelength instabilities growing on a counter-rotating Lamb-Oseen vortex pair for small  $a/b$ . The following sections describe the instability growth in the vortex pair as the separation distance is changed.

### 9 Instability growth rate

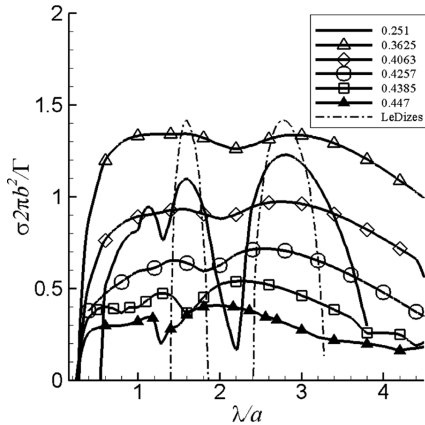
The growth rate of the leading instability mode was monitored. For each case a disturbance was introduced characterised by its wave-number

$$k = 2\pi/\lambda, \tag{13}$$

where  $\lambda$  is the axial wavelength of the disturbance. The wave-number  $k$  was changed such that results were taken at consistent values of normalised wavelength  $\lambda/a$ .

Figure 7 shows a comparison of the linear growth rate of elliptical instabilities as a function of the normalised axial wavelength, over different separation ratios  $a/b$ . The number of principal modes evident in each separation case varies as the non-uniform strain field acts to enhance or suppress instability modes. At a separation of  $a/b = 0.251$  three principal modes are evident. The first has a peak growth rate at  $\lambda/a = 1.15$ , this peak was not reported by Le Dizès and Laporte (2002). The remaining peaks occur at  $\lambda/a = 1.6$  and at  $\lambda/a = 2.8$ . The positions of this peak growth rate correlate with Le Dizès and Laporte’s (2002) results for  $a/b = 0.18$  at  $Re = \infty$ , also shown in Figure 5.

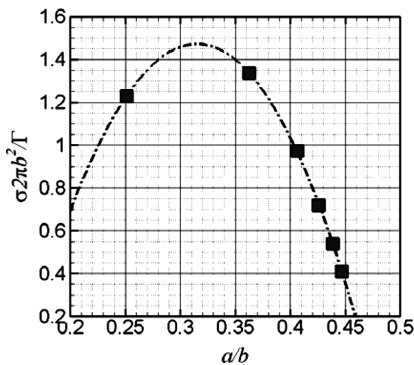
**Figure 7** Growth rate of the elliptical instability as a function of the normalised axial wave-number; --- from Le Dizès and Laporte (2002), results for  $a/b = 0.18$  and  $Re = \infty$ . Legend describes  $a/b$  ratio



The significant finding shown in Figure 7 is that at closer vortex spacing the growth rate at all wavelengths is enhanced, relative to the peak growth rate. In addition we note the damping out of the  $\lambda a = 1.15$  peak found in  $a/b = 0.251$ . It is observed that in distantly separated cases the peak growth rates are sharp and well defined. As the vortices are brought closer together however, each peak broadens.

Critical wave-lengths, where a local peak in growth rate is observed, decrease as the distance between vortices decreases. The strongest mode is at  $\lambda a = 2.8$  at a separation distance of  $a/b = 0.251$  but decreases to  $\lambda a = 1.8$  at  $a/b = 0.447$ , this is observed as a lateral shifting of the peak structures in Figure 7. Furthermore, the growth rates of the instabilities vary with vortex separation. Figure 8 shows the normalised growth rate of the peak instability mode in each separation case. It can be seen that after an initial increase in growth rate, the growth rate of the peak instability mode decreases as the vortices are brought closer together. This is in contrast to the findings of Lewke and Williamson (1998) who postulate that bringing vortices closer together enhanced the growth rate of the  $[-1, 1]$  Kelvin mode. By contrast our results find an optimum separation distance.

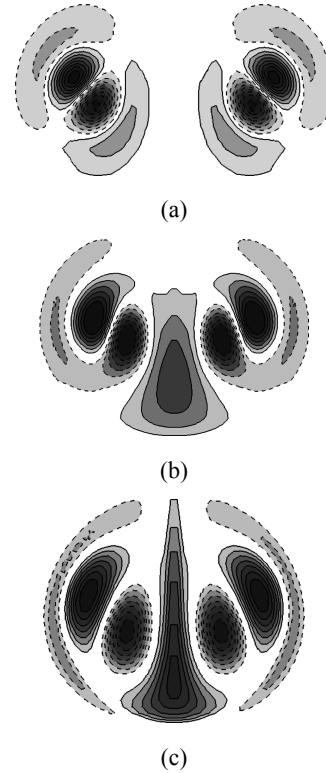
**Figure 8** Normalised growth rate of peak instability mode as a function of vortex separation distance



### 10 Coupling of vortices

Figure 9 shows the perturbation fields of the dominant instability modes for a range of  $a/b$ . The images are created by subtracting two slices of the vorticity field half a period out of phase. The positive and negative vorticity in Figure 9 are the same structure at different points in the stream tube.

**Figure 9** Contours of the vorticity field mode-shapes taken at the peak growth rate: (a)  $a/b = 0.251$ ; (b)  $a/b = 0.3625$  and (c)  $a/b = 0.4385$ . Dashed contours represent negative vorticity



At large separation distances, (Fig. 9(a)), the perturbation vorticity field in each vortex stream tube comprises two distinct regions. An inner region exists of high perturbation vorticity that sits within the characteristic core radii, and a less intense outer region that curls around in a crescent shape offset from the vortex core. These may be analysed as a pair of co-rotating perturbation vortices formed in each stream tube of the perturbation field. Figure 10 shows a three dimensional representation of the perturbation field for  $a/b = 0.251$ . This mode shape is typical of the first branch of the Kelvin mode  $[-1, 1]$  (for example see Waleffe, 1990).

As the two base vortices are brought closer together, the outer perturbation vortex structures from each stream tube undergo vortex merging, coupling the perturbation vortices. This region, referred to herein as the central coupled region, spikes up sharply along the centreline between the stream tubes. This occurs because the stream tubes are close enough for each of the outer co-rotating vortices to merge, forming a single perturbation vortex core

(Fig. 11). The correlation between the periodic nature of the convergence and the phase of the disturbance indicates a direct relationship between the procession rate of the co-rotating vortices and the disturbance frequency.

**Figure 10** Three dimensional extrapolation of the perturbation vorticity field at relatively distant vortex spacing  $a/b = 0.251$ . Vorticity of each iso-surface is  $\omega_z = 4.0$ . Note the sinusoidal nature of the perturbation fields with the pairs of vortices seen in Figure 9(a)



**Figure 11** Three dimensional extrapolation of the perturbation vorticity field at vortex spacing  $a/b = 0.447$ . Each iso-surface is  $\omega_z = 0.28$ . Note the merged vortex structure in 3D which corresponds to the structure of Figure 10(b)–(c)



As the base vortex pair is brought still closer together (Fig. 9(c)), we see an increase in the relative strength of the central coupled region compared to the maximum perturbation vorticity in the vortex plane. This is shown in the progression of contours in Figure 9(a)–(c). The relative increase in the strength of the central coupled region with respect to the vortex core region amplifies the coupling effect.

## 11 The complete three dimensional field

Figure 12 shows a three dimensional reconstruction of the complete flow field, defined as the addition of the base field to the perturbation field multiplied by an arbitrary value. It shows a periodic crossover of fluid between the each vortex in the pair. This is observed as small bulges emanating from the vortex stream tubes. These features are better developed in Figure 12(a) where the vortices are closely spaced. These structures are evident at both close and distant separations, however at the distant separation a resolution 31 times greater is required for them to be seen.

Leweke and Williamson (1998) and Ryan and Sheard (2007) showed that growing deformations of the short-wave instabilities give rise to periodic cross-over of fluid between vortices. This creates an array of secondary vortices perpendicular to the primary pairs, which quickly lead to the breakdown of primary vortex circulation. In Figure 12 we see the growth of the periodic fluid cross-over regions. These form as the central coupled region of the perturbation

field acts to draw the fluid from each base vortex stream tube across to the other vortex. Experimentally this has only been observed during the non-linear growth period and has not been described numerically or analytically. However this analysis shows that it is in fact due to the principal linear growth mode. We postulate that the growth of the fluid crossovers and eventual secondary vortex production are accelerated by the non-linear growth regime as well as by close proximity of the vortices. In either case this allows coupling of the perturbation vorticity field (shown in Fig. 9).

**Figure 12** Three dimensional reconstructions of axial vorticity iso-surfaces with fluid crossover regions shown: (a)  $a/b = 0.447$  and (b)  $a/b = 0.251$



## 12 Conclusions

This investigation has considered the growth of short-wave elliptical instabilities in a Lamb-Oseen vortex pair subject to non-uniform strain fields at close vortex spacing, using DNS. Previous research has been conducted at relatively large vortex spacing, where the mutually induced strain field that causes the elliptical deformation of vortex cores is typically uniform. This study investigated the instability growth over a range of wave-numbers as the vortex spacing is reduced.

A limit of minimum vortex spacing was found via a viscous diffusion method previously employed by Le Dizès and Verga (2002). A counter-rotating vortex pair with equal circulation magnitude may not exist closer than a separation ratio of  $a/b = 0.5$ . This indicates that the vortex pair exerts a mutual force on each vortex such that invariant streamlines may not overlap.

The perturbation analysis of the vortices was conducted by developing linear modes over a frozen base flow. It was found that as vortex spacing is reduced, the growth rate of non-principal wave-numbers is enhanced relative to the principal wave-numbers. The peak growth rate of the principal instability mode reduced as the vortices were brought closer together. At other wave-numbers, the growth rate increased relative to the peak, resulting in a broadening of the growth rate profile.

The perturbation field was shown to be composed of a pair of co-rotating vortices in each stream tube, which could merge at close vortex spacing to cause coupling of the vortex stream tubes in the fluid cross over region. These fluid cross over regions, which were shown to be products of a linear growth regime, were shown to exist at large separations but were greatly enhanced at close separations.

The dissipation of vortex pairs is an important field of study for the aviation industry, in which enhanced vortex dissipation may lead to increased efficiency of air infrastructure. It should, therefore, be considered in future wing design.

## References

- Bayly, B.J. (1986) 'Three dimensional instability of elliptical flow', *Phys. Rev. Lett.*, Vol. 57, pp.2160–2163.
- Bayly, B.J., Orszag, S.A. and Herbert, T. (1988) 'Instability mechanisms in shear-flow transition', *Annu. Rev. Fluid Mech.*, Vol. 20, pp.359–391.
- Blackburn, H.M. and Sheard, G.J. (2010) 'On quasi-periodic and subharmonic Floquet wake instabilities', *Physics of Fluids*, Vol. 22, No. 3, pp.031701:1–4.
- Crow, S.C. (1970) 'Stability theory for a pair of trailing vortices', *AIAA J.*, Vol. 8, pp.2172–2179.
- Eloy, C., Le Gal, P. and Le Dizès, S. (2003) 'Elliptic and triangular instabilities in rotating cylinders', *J. Fluid Mech.*, Vol. 476, pp.357–388.
- Karniadakis, G.E., Israeli, M. and Orszag, S.A. (1991) 'High-order splitting methods for the incompressible Navier-Stokes equations', *J. Comput. Phys.*, Vol. 97, No. 2, pp.414–443.
- Le Dizès, S. and Laporte, F. (2002) 'Theoretical predictions for the elliptical instability in a two-vortex flow', *J. Fluid Mech.*, Vol. 471, pp.169–201.
- Le Dizès, S. and Verga, A. (2002) 'Viscous interactions of two co-rotating vortices before merging', *J. Fluid Mech.*, Vol. 467, pp.389–410.
- Leweke, T. and Williamson, C.H.K. (1998) 'Cooperative elliptic instability in a vortex pair', *J. Fluid Mech.*, Vol. 360, pp.85–119.
- Meunier, P. and Leweke, T. (2005) 'Elliptic instability of a co-rotating vortex pair', *J. Fluid Mech.*, Vol. 33, pp.125–159.
- Moore, D.W. and Saffman, P.G. (1975) 'The instability of a straight vortex filament in a strain field', *Proc. R. Soc. Lond. A*, Vol. 346, pp.413–425.
- Olwi, I. and Ghazi, M. (1992) 'Effect of wing tip vortices on a trailing aircraft', *AIAA J.*, Vol. 30, pp.2186–2187.
- Phillips, F. (2004) *Mechanics of Flight*, Wiley and Sons, Hoboken New Jersey.
- Pierrehumbert, R.T. (1986) 'Universal short-wave instability of two dimensional eddies in an inviscid fluid', *Phys. Rev. Lett.*, Vol. 57, pp.2157–2160.
- Ryan, K. and Sheard, G.J. (2007) 'Non-linear growth of short-wave instabilities in a Batchelor vortex pair', in Jacobs, P., McIntyre, T., Cleary, M., Buttsworth, D., Mee, D., Clements, R., Morgan, R. and Lemckert, C. (Eds.): *Proceedings of the 16th Australasian Fluid Mechanics Conference*, Pub: School of Engineering, The University of Queensland, ISBN: 978-1-864998-94-8, Crown Plaza, Gold Coast, Queensland, Australia, 3–7 December, pp.1463–1469.
- Sheard, G.J., Fitzgerald, M.J. and Ryan, K. (2009) 'Cylinders with square cross section: wake instabilities with incidence angle variation', *Journal of Fluid Mechanics*, Vol. 630, pp.43–69.
- Sheard, G.J., Leweke, T., Thompson, M.C. and Hourigan, K. (2007) 'Flow around an impulsively arrested circular cylinder', *Physics of Fluids*, Vol. 19, No. 8, pp.083601:1–14.
- Sipp, D., Jacquin, L. and Cossu, C. (2000) 'Self-adaptation and viscous selection in concentrated two dimensional dipoles', *Phys. Fluids*, Vol. 12, pp.245–248.
- Spalart, P. (1998) 'Airplane trailing vortices', *Annu. Rev. Fluid Mech.*, Vol. 30, pp.107–138.
- Tsai, C-Y. and Widnall, S.E. (1976) 'The stability of short waves on a straight vortex filament in a weak externally imposed strain field', *J. Fluid Mech.*, Vol. 73, pp.721–733.
- Waleffe, F. (1990) 'On the three dimensional instability of strained vortices', *Phys. Fluids A*, Vol. 2, p.76.